Determination of Pore-Scale Transverse Dispersivity by Taylor-Aris Dispersion in a Helical Soil Column

M. A. Rahman[1], I. Benekos[2], O.A. Cirpka[1], P.K. Kitanidis[2]

[1]Universität Stuttgart, Institut für Wasserbau, Pfaffenwaldring 61, 70550 Stuttgart, Germany, Arifur.Rahman@iws.uni-stuttgart.de; Olaf.Cirpka@iws.uni-stuttgart.de.

[2]Stanford University, Dept. of Civil and Environ. Eng. Terman. Engineering Center, Stanford, CA 95305-4020 USA, ybenekos@stanford.edu, peterk@stanford.edu.

Abstract. A concise methodology for determining the pore scale transverse dispersion parameters of saturated porous medium in a laboratory column experiments is developed. We use a specially designed helical column filled with glass beads. The geometry of the helix causes velocity differences in the radial direction which cause angular spreading of the solutes. The resulting longitudinal macrodispersion follows the principles of Taylor-Aris dispersion, in which the longitudinal macrodispersion is inversely proportional to local transverse dispersion coefficient. We introduce a conservative tracer continuously into the helix, measure the breakthrough curve in the outflow, and analyze its temporal moments. Multiple tracer experiments with different discharge rates are conducted. We estimate the local transverse dispersion parameters using analytical expressions for the angular macrodispersion coefficient in the large-time limit and numerical methods for the angular macrodispersion coefficient accounting for the entire time range. The method presented here offers a new perspective for investigating pore-scale transverse dispersion parameters in porous media.

Introduction

Pore-scale dispersion plays a decisive role in the decay of concentration fluctuations, dilution of conservative solutes, and mixing of reacting compounds [Kitanidis, 1994; Cirpka and Kitanidis, 2000; Attinger et al., 1999]. Although pore scale transverse dispersivities are much smaller (for medium sand $\approx 10^{-4}$ m) than the related longitudinal dispersivities, the mixing due to transverse dispersion controls, under certain conditions, the reactive behavior of interacting compounds in heterogeneous media.

The objective of the study is to develop a novel method for the determination of pore-scale transverse dispersion parameters that are difficult to obtain with the existing methods. We use a helical device (see Figure 1) the geometry of which induces shear flow in isotropic, homogeneous porous media. Applying a head difference between the inlet and outlet of the helix, the angular velocities are higher at the inside of the helix than at the outside. When a conservative solute is introduced, velocity differences lead to angular spreading of the solutes. The breakthrough curve of the flux-averaged concentration in the outflow of the helix spreads inversely proportional to the local transverse dispersion coefficient. This is in contrast to most existing methods for the determination of transverse dispersion (e.g. Grane and Gardner [1961]; Robbins [1989]) in which a quantity is measured that is proportional to the dispersion coefficient.

Theory

Taylor-Aris Dispersion

In any type of shear flow, where the magnitude of the velocity varies normal to its orientation, the asymptotic longitudinal macrodispersion coefficient is proportional to the mean velocity squared and inversely proportional to the transverse diffusion coefficient. This has been analyzed first for transport in

a capillary tube with laminar flow by Taylor [1953] and Aris [1956]. Cirpka and Kitanidis [2001] have analyzed the same type of macrodispersion for a helical device by the method of spatial moments. In the present study we consider the temporal moments as obtained from a breakthrough curve in the outflow of the helix.

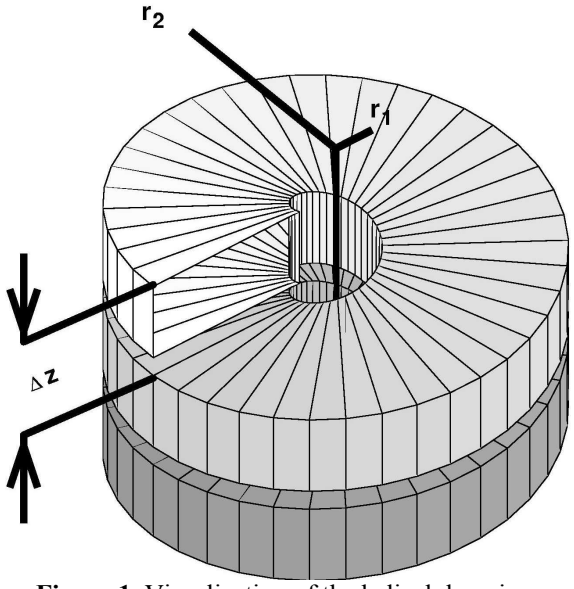

Figure 1. Visualization of the helical domain.

Flow and Transport Equations in a Helical Porous Medium

We consider a helical domain as shown in Figure 1. The domain is characterized by the inner and outer radius r_1 and r_2, the pitch Δz, and the number of convolutions n. A head difference is applied between the inlet and outlet cross sections. If we assume that Δz is negligible in comparison to the radii and if we consider quantities that are averaged over the thickness of one whorl the flow can be viewed as two-dimensional and the helix would simplify to a ring. In a ring, the angular coordinate φ ranges only from 0 to 2π. For a small pitch $\Delta z > 0$ though many rotations are possible thus forming the helix. In our theoretical analysis, the helix is semi-infinite and ranges from 0 to $+\infty$.

Applying a constant head at the in- and outflow faces, the specific discharge components are:

$$q_r = 0 \qquad (1), \qquad q_\varphi = \frac{KJ}{r} \qquad (2)$$

where r and φ are the radial and angular coordinates, K is the hydraulic conductivity, and J is the negative angular head gradient. The corresponding transport equation for a negligible pitch $\Delta z \to 0$ is [Cirpka and Kitanidis, 2001]:

$$\frac{\partial c}{\partial t} + \frac{q_\varphi}{r\theta}\frac{\partial c}{\partial \varphi} - \frac{D_l}{r^2}\frac{\partial^2 c}{\partial \varphi^2} - \frac{\partial}{\partial r}\left(D_t \frac{\partial c}{\partial r}\right) - \frac{D_t}{r}\frac{\partial c}{\partial r} = 0 \qquad (3)$$

subject to the boundary conditions:

$$\left.\frac{\partial c}{\partial r}\right|_{r=r_1, r_2} = 0 \qquad (4), \qquad c(\varphi=0) = \delta(t) \qquad (5)$$

where c is the concentration in the aqueous phase, θ is the effective porosity, t is time and D_l and D_t are the longitudinal (tangential) and transverse (radial) dispersion coefficients, respectively [Scheidegger, 1961]:

$$D_l = \alpha_l \frac{q_\varphi}{\theta} + D \qquad (6), \qquad D_t = a_t \frac{q_\varphi}{\theta} + D \qquad (7)$$

in which α_l and α_t are the longitudinal and transverse dispersivities which are properties of the porous medium, and D is the effective diffusion coefficient which may differ from the molecular by a factor referred to as tortuosity. At the large-distance limit we impose the auxiliary condition:

$$\lim_{\varphi \to +\infty} \frac{\partial^n c(\varphi, r, t)}{\partial \varphi^n} = 0 \quad \forall n \geq 0 \qquad (8)$$

Temporal Moments

The k-th temporal moment of the flux-weighted concentration is defined as:

$$M_k(\varphi) = \frac{1}{Q_{tot}} \int_{r_1}^{r_2} q_\varphi(r) \int_0^\infty t^k c(t, r, \varphi) dt dr \qquad (9)$$

with:

$$Q_{tot} = \int_{r_1}^{r_2} q_\varphi(r) dr (\Delta z - z_f) = KJ \ln\left(\frac{r_2}{r_1}\right)(\Delta z - z_f) \qquad (10)$$

which is the total discharge and $(\Delta z\text{-}z_f)$ is the height of the cross-section. For the second and higher moments we also define central moments $M_{kc}(\varphi)$:

$$M_{kc}(\varphi) = \frac{1}{Q_{tot}} \int_{r_1}^{r_2} \int_0^\infty \left(t - \frac{M_1}{M_2}\right)^k \frac{c(t, r, \varphi)}{r} dt dr \qquad (11)$$

In analogy to transport in parallel flow, we expect that the flux-weighted cross-sectional average of the concentration satisfies, after a relaxation time, a macroscopic advection-dispersion equation:

$$\frac{\partial \breve{c}}{\partial t} + \omega_{mac} \frac{\partial \breve{c}}{\partial \varphi} - D^\varphi_{mac} \frac{\partial^2 \breve{c}}{\partial t^2} = 0 \qquad (12)$$

with the flux-weighted concentration $\breve{c}$:

$$\breve{c}(\varphi, t) = \frac{1}{\ln\left(\frac{r_2}{r_1}\right)} \int_{r_1}^{r_2} \frac{c(r, \varphi, t)}{r} dr \qquad (13)$$

ω_{mac} and D^φ_{mac} are the macroscopic rotational seepage velocity and dispersion coefficient respectively. These macroscopic parameters can be expressed in terms of the dimensions r_1 and r_2 of the helix, the total specific discharge Q_{tot}, the porosity θ, and the parameters determining pore-scale dispersion α_l, α_t, and D. We relate the angular derivatives of the global moments to the macroscopic parameters ω_{mac} and D^φ_{mac} by:

$$\frac{\partial M_0}{\partial \varphi} = 0 \quad (14), \qquad \frac{\partial M_1}{\partial \varphi} = \frac{M_0}{\omega} \quad (15), \qquad \frac{\partial M_{2c}}{\partial \varphi} = \frac{2D_{mac}^{\varphi}}{\omega^3} M_0 \quad (16)$$

By applying the method of temporal moments, the mean rotational seepage velocity is obtained as:

$$\omega = \frac{2Q_{tot}}{\theta\left(r_2^2 - r_1^2\right)\left(\Delta z - z_f\right)} \tag{17}$$

At the large-distance limit, we can derive the macrodispersion coefficient in a closed form for the limiting cases of a) no molecular diffusion and b) only molecular diffusion. For a derivation of the closed form of the macrodispersion coefficient please refer to Cirpka and Kitanidis [2001].

a) By neglecting the transverse dispersivity, $\alpha_t = 0$ ($\Rightarrow D_t = D$), we obtain:

$$\lim_{\varphi\to\infty}\frac{\partial M_{2c}}{\partial \varphi} = \frac{\left(\Delta z - z_f\right)\theta}{Q_{tot}} \frac{r_2^4\left(4\left(\ln\frac{r_2}{r_1}\right)^2 - 9\ln\frac{r_2}{r_1} + 6\right) + r_2^2 r_1^2\left(4\left(\ln\frac{r_2}{r_1}\right)^2 - 12\right) + r_1^4\left(4\left(\ln\frac{r_2}{r_1}\right)^2 + 9\ln\frac{r_2}{r_1} + 6\right)}{24\ln\left(\frac{r_2}{r_1}\right) D} \tag{18}$$

b) By neglecting the molecular diffusion, $D = 0$ ($\Rightarrow D_t = \alpha_t q_\varphi$), we obtain:

$$\lim_{\varphi\to\infty}\frac{\partial M_{2c}}{\partial \varphi} = \frac{\theta^2\left(\Delta z - z_f\right)^2}{Q_{tot}^2} \frac{\left(\frac{4}{15}\left(r_2^5 - r_1^5\right)\ln\left(\frac{r_2}{r_1}\right)^2 + \frac{8}{9}\left(r_1^2 r_2^3 - r_2^5 + r_1^3 r_2^2 - r_1^5\right)\ln\left(\frac{r_2}{r_1}\right) + r_2^5 - r_1 r_2^4 - 2r_1^2 r_2^3 + 2r_1^3 r_2^2 + r_1^4 r_2 - r_1^5\right)}{\alpha_t \ln\left(\frac{r_2}{r_1}\right)} \tag{19}$$

Neglecting the effect of the early-time behavior on the value of M_{2c}, we get the following general relationship between M_{2c} at a given φ and Q_{tot}:

$$M_{2c}\left(D, 0, Q_{tot}\right) = \frac{B}{Q_{tot}} \quad (20), \qquad M_{2c}\left(0, \alpha_t, Q_{tot}\right) = \frac{A(r_1, r_2, \alpha_t)}{Q_{tot}^2} \quad (21)$$

We can approximate the combined effects of D and α_t by considering that the local dispersion contributions are additive and the macrodispersion is inversely proportional to transverse dispersion. Therefore we use the approximation:

$$\frac{1}{Q_{tot} M_{2c}\left(D, \alpha_t, Q_{tot}\right)} \approx \frac{1}{B} + \frac{Q_{tot}}{A} \tag{22}$$

Experimental Column Design and Methodology

The helix is manufactured in stainless steel. It has 60 rotations. The outer diameter is 10 cm, the core diameter 3 cm, and the pitch has a value of 27 mm. The thickness of the flights is 2 mm, so that the effective thickness of the packing is 25 mm. The packing consists of glass beads with a grain size of 0.75 mm -1 mm. The porosity is ≈40%.

Fluorescein is used as conservative tracer. It is detected by fiber-optic probes at the in- and outlet of the helix. Fluorescein was dissolved in deionized water at a concentration of 500µg/l. Sodium hydroxide was added to the tracer solution in order to adjust the pH to a value of 9 at which Flourescein gives

the highest intensity of fluorescence. The fiber-optic probes were connected to a Fluorometer, and a personal computer was used for continuous data acquisition.

To prevent reduction of the hydraulic conductivity by entrapped gas, the unsaturated column was first flushed with gaseous carbon dioxide and subsequently with degassed water dissolving all gas.

A constant discharge was applied by a head difference between the in- and outlet of the helix. Starting at some time t_0, the tracer solution was injected continuously into the porous medium. We measured the breakthrough curve at the outflow of the helix. Due to the velocity profile, the concentrations at the inner radius of the cross section contribute more to the mean mass flux than those at the out radius. Therefore, the measured concentration is flux-averaged.

Results and Data Analysis

Five experiments were conducted each with different discharge rate to distinguish the contributions of molecular diffusion and hydrodynamic to transverse dispersion. The measured concentrations were normalized by the inflow concentration, so that the concentration values in the breakthrough curves, shown in Figure 2, range from zero to one.

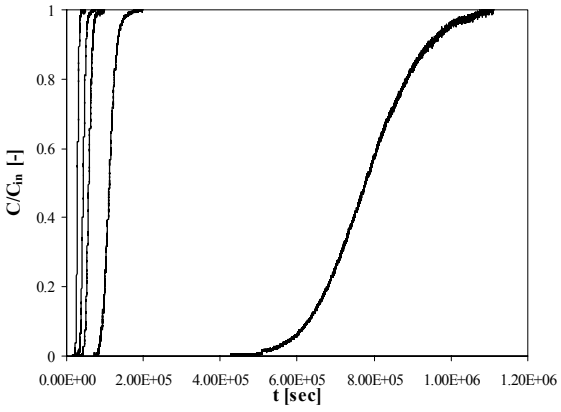

Figure 2: Normalized breakthrough curves as a function of real time for the different experiments

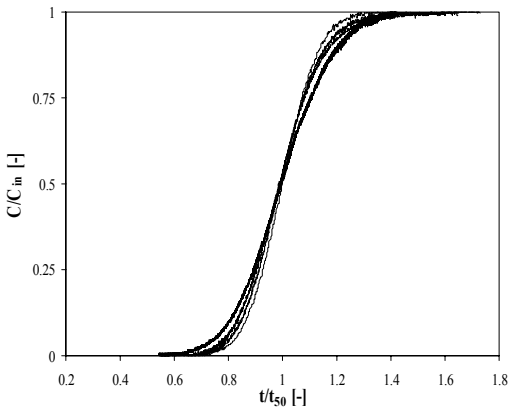

Figure 3: Normalized concentration breakthrough curves plotted in a normalized time axis. The time axis is normalized by the mean arrival time t_{50} of the tracer front.

The time length of the experiments ranged from a few hours to several days. Figure 3 shows the concentration breakthrough curves in dimensionless axes. Here, the time is divided by the mean arrival time of the concentration front denoted by t_{50}. The curve in Figure 3 with the most spreading refers to the experiment with the lowest discharge rate (experiment 5 in Table 1), and the curve with the least spreading to that with the highest discharge rate (experiment 1 in Table 1). That is, the macroscopic Péclet number $Pe_{mac} = \omega_{mac}\varphi/D^{\varphi}_{mac}$ increases with discharge rate.

The apparent macroscopic parameters D^{φ}_{mac} and ω_{mac} were evaluated by fitting the analytical solution of Ogata and Banks [1961] for the Heaviside problem to the measured data. From the fitted macroscopic parameters, we derived the temporal moments M_{2c} and M_1 by using eqns (15) and (16) and compared them to the moments calculated directly from the breakthrough curves. The comparison gave us a measure for the error in M_{2c} and M_1. The effective porosity n_e was calculated by $\theta = \Omega / \omega_{mac}$ in which Ω is the angular rotational specific discharge:

$$\Omega = \frac{2KJ \ln\left(\frac{r_2}{r_1}\right)}{r_2^2 - r_1^2} \tag{23}$$

As listed in Table 1, the estimated first moment M_1 has an error < 1% for all experiments except experiment 5 where it has a value of 2.67%. As a consequence, we got consistent estimates of the porosity. Similarly, the second central moment M_{2c} could be estimated quite accurately (relative error < 10%) except in experiment 5 where more time should have been allowed in order to capture the full tail of the breakthrough curve.

Table 1: Parameters calculated from the different experiments

Parameter	**Experiment number**				
	1	**2**	**3**	**4**	**5**
Total Discharge, Q_{tot} [m^3/s]	$1.5*10^{-7}$	$1.0*10^{-7}$	$7.5*10^{-8}$	$3.83*10^{-8}$	$5.55*10^{-9}$
First Moment, M_1 [s]	$2.88*10^{4}$ ±0.25%	$4.38*10^{4}$ ±0.20%	$5.82*10^{4}$ ±0.57%	$1.12*10^{5}$ ±2.67%	$7.89*10^{5}$ ±0.12%
Second Central Moment, M_{2c} [s^2]	$9.78*10^{6}$ ±9.6%	$2.96*10^{7}$ ±6.4%	$5.18*10^{7}$ ±4.8%	$2.31*10^{8}$ ±9.0%	$1.64*10^{10}$ ±25.0%
Angular Rotational Specific Discharge, Ω [1/s]	0.0053	0.0035	0.0026	0.0013	0.00019
Macroscopic Rotational Velocity, ω_{mac} [1/s]	0.0131	0.0086	0.0065	0.0034	0.00048
Macroscopic Angular Dispersion Coefficient, D^{φ}_{mac} [1/s]	0.0290	0.0251	0.0181	0.0116	0.0024
Macroscopic Peclet Number [-]	170	129	131	109	76
Effective Porosity, θ [-]	0.403	0.408	0.407	0.401	0.405

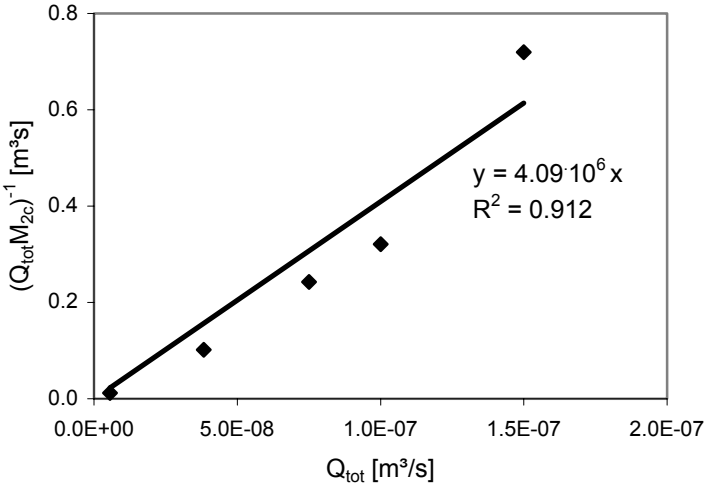

Figure 4: Linear regression of $(Q_{tot}M_{2c})^{-1}$ as a function of Q_{tot} for the given data.

Figure 4 shows a linear regression of $(Q_{tot}M_{2c})^{-1}$ as a function of Q_{tot} for the measured data. Obviously, coefficients A and B of eq. (22) are the inverse of the slope and the intercept of the regression line. Considering eqns. (20) and (21), we can approximate D and α_t from A and B by:

$$D = \frac{\Delta\varphi}{B}\theta \frac{r_2^4\left(4\left(\ln\frac{r_2}{r_1}\right)^2 - 9\ln\frac{r_2}{r_1} + 6\right) + r_2^2 r_1^2\left(4\left(\ln\frac{r_2}{r_1}\right)^2 - 12\right) + r_1^4\left(4\left(\ln\frac{r_2}{r_1}\right)^2 + 9\ln\frac{r_2}{r_1} + 6\right)}{24\ln\left(\frac{r_2}{r_1}\right)} \tag{25}$$

$$\alpha_t = \frac{\Delta\varphi}{A}\theta^2 \frac{\left(\frac{4}{15}\left(r_2^5 - r_1^5\right)\ln\left(\frac{r_2}{r_1}\right)^2 + \frac{8}{9}\left(r_1^2 r_2^3 - r_2^5 + r_1^3 r_2^2 - r_1^5\right)\ln\left(\frac{r_2}{r_1}\right) + r_2^5 - r_1 r_2^4 - 2r_1^2 r_2^3 + 2r_1^3 r_2^2 + r_1^4 r_2 - r_1^5\right)}{\ln\frac{r_2}{r_1}} \tag{26}$$

The discharge rates were fairly high in all experiments. At these rates, molecular diffusion contributed marginally to local transverse dispersion. As a consequence, we were not able to estimate D from the data. In fact, the intercept of the regression was negative. That is, we could determine only the value of the transverse dispersivity.

As noted above, eqns. (20) and (21) refer to the large-distance limit. Therefore, early-time effects on M_{2c} are neglected in the regression-based analysis. We used the resulting values α_t and D as initial guess in a Gauss-Newton scheme that uses a numerical solution of the moment-generating equations accounting for the entire time range. Table 2 shows the initial guess for parameters α_t, D, and θ as well as their final estimates computed by the Gauss-Newton method. As in the regression-based analysis, we were not able to determine the diffusion coefficient from the data.

Table 2: Initial guess and final estimate for parameters D, α_t, and θ.

Parameter	**Initial guess**	**Final estimate**
D [m^2/s]	Set to 0	Set to 0
α_t [m]	$7.27*10^{-4}$	$6.57*10^{-4}$
θ	0.404	0.405

Discussion, Conclusions, and Future Work

The presented method for the determination of pore-scale transverse dispersion coefficients is based on Taylor-Aris dispersion. We measure the spread of the breakthrough curve which is inversely proportional to the local transverse dispersion coefficient. This is advantageous, because transverse-dispersion parameters are generally small.

The experimental results obtained so far did not meet all of our expectations. We wanted to distinguish between the velocity-dependent and –independent contributions to pore-scale transverse dispersion. With the chosen discharge rates, this was not possible. We will therefore conduct additional experiments at lower flow rates.

As shown in Figure 4, $(Q_{tot}M_{2c})^{-1}$ does not depend linearly on Q_{tot}. To a certain extent, this might be contributed by early-time effects. An alternative interpretation could be that the hydrodynamic contribution to pore-scale transverse dispersion is not a linear function of the velocity. Our data could be fitted much better by a power-law regression with an exponent of ≈1.2. This exponent has

been observed previously in experiments on longitudinal pore-scale dispersion [Bear, 1972]. We will therefore extend the numerical scheme to include the exponent assigned to the velocity in the parameterization of transverse dispersion as fitting parameter.

The transverse-dispersion coefficients determined by our analysis are higher than expected. Our analysis is based on the assumption that the three-dimensionality of flow due to the pitch of the helix can be neglected. A more detailed analysis of the flow field in the helix may show whether this assumption affects the measured Taylor dispersion. As the slope of the domain varies with the radius, there might be secondary motion, that is, circular flow within the cross-section adding to the main flow parallel to the walls. In this case, transverse dispersion is no more the only process exchanging solute mass between the inside, where the flow is fast, and the outside of the helix, where flow is slow. We will investigate whether secondary motions exists and how it eventually influences longitudinal macrodispersion. For this purpose, we will perform both theoretical studies and three-dimensional simulations.

References

Aris, R., On the dispersion of a solute in a fluid flowing through a tube, *Proc. R. Soc. Londo*n, *Ser.* A, *235*, 67–77, 1956.

Attinger, S., M. Dentz, H. Kinzelbach, and W. Kinzelbach, Temporal behavior of a solute cloud in a chemically heterogeneous porous medium, *J. Fluid Mec*h., *386*, 77–104, 1999.

Bear, J., *Dynamics of Fluids in Porous Media*, chapter 10: Hydrodynamic Dispersion, pp. 579-663. American Elsevier, New York, 1972.

Cirpka, O. A., and P. K. Kitanidis, Theoretical basis for the measurement of local transverse dispersion in isotropic porous media, *Water Resour. Re*s., *3*7(2), 243–252, 2001.

Cirpka, O. A., and P. K. Kitanidis, Characterization of mixing and dilution in heterogeneous aquifers by means of local temporal moments, *Water Resour. Re*s., *3*6(5), 1221–1236, 2000.

Grane, F. E., and G. H. F. Gardner, Measurements of transverse dispersion in granular media, *J. Chem. Eng. Dat*a, 6(2), 283–287, 1961.

Kitanidis, P. K., The concept of the dilution index, *Water Resour. Re*s., *3*0(7), 2011–2026, 1994.

Kreft, A., and Zuber, A., On the physical meaning of the dispersion equation and its solutions for different initial and boundary conditions. Chem. Eng. Sc. 33:1471-1480, 1971

Ogata, A., and Banks, R.B., A solution of the differential equation of longitudinal dispersion in porous media. U.S. Geol. Surv. Prof. Paper 411-A, 1961

Robbins, G. A., Methods for determining transverse dispersion coefficients of porous media in laboratory column experiments, *Water Resour. Re*s., *2*5(6), 1249–1258, 1989.

Scheidegger, A.E., General theory of dispersion in liquid flow through porous media, J. Geophys. Res., 66(10), 3273-3278, 1961

Taylor, G. I., Dispersion of soluble matter in solvent flowing slowly through a tube, *Proc. R. Soc. Londo*n, *Ser.* A, *219*, 186–203, 1953.